

## Using Temporal Changes in Drought Indices to Generate Probabilistic Drought Intensification Forecasts

JASON A. OTKIN

*Cooperative Institute for Meteorological Satellite Studies, University of Wisconsin–Madison, Madison, Wisconsin*

MARTHA C. ANDERSON

*Hydrology and Remote Sensing Laboratory, Agricultural Research Services, U.S. Department of Agriculture, Beltsville, Maryland*

CHRISTOPHER HAIN

*Earth System Interdisciplinary Center, University of Maryland, College Park, College Park, Maryland*

MARK SVOBODA

*National Drought Mitigation Center, University of Nebraska–Lincoln, Lincoln, Nebraska*

(Manuscript received 20 March 2014, in final form 22 July 2014)

### ABSTRACT

In this study, the potential utility of using rapid temporal changes in drought indices to provide early warning of an elevated risk for drought development over subseasonal time scales is assessed. Standardized change anomalies were computed each week during the 2000–13 growing seasons for drought indices depicting anomalies in evapotranspiration, precipitation, and soil moisture. A rapid change index (RCI) that encapsulates the accumulated magnitude of rapid changes in the weekly anomalies was computed each week for each drought index, and then a simple statistical method was used to convert the RCI values into drought intensification probabilities depicting the likelihood that drought severity as analyzed by the U.S. Drought Monitor (USDM) would worsen in subsequent weeks. Local and regional case study analyses revealed that elevated drought intensification probabilities often occur several weeks prior to changes in the USDM and in topsoil moisture and crop condition datasets compiled by the National Agricultural Statistics Service. Statistical analyses showed that the RCI-derived probabilities are most reliable and skillful over the central and eastern United States in regions most susceptible to rapid drought development. Taken together, these results suggest that tools used to identify areas experiencing rapid changes in drought indices may be useful components of future drought early warning systems.

### 1. Introduction

Drought is an intrinsic feature of the climate system that adversely affects the economy and can lead to substantial social displacements owing to job losses and lower economic output. During the past decade, severe drought conditions have enveloped large areas of the United States, with some regions remaining entrenched in drought for many years. According to the U.S. Drought Monitor

(USDM; <http://droughtmonitor.unl.edu/>) (Svoboda et al. 2002), at the peak of the 2012 drought, over 80% of the contiguous United States (CONUS) was characterized by abnormal dryness, with nearly half of the country experiencing from severe (D2) to exceptional (D4) drought conditions. The extreme drought severity led to substantial yield losses for grain farmers in the Corn Belt and to smaller livestock herds in the south-central United States, as ranchers were forced to sell or relocate animals owing to a lack of forage and high feed prices. Federal crop indemnity payments for 2012 exceeded \$17 billion (USDA 2013), with the total cost of the drought estimated to surpass \$35 billion (Aon Benfield 2013), making it one of the most expensive natural disasters in U.S. history. The

*Corresponding author address:* Jason A. Otkin, Cooperative Institute for Meteorological Satellite Studies, University of Wisconsin–Madison, 1225 W. Dayton St., Madison, WI 53706.  
E-mail: jason.otkin@sscc.wisc.edu

high economic cost combined with other societal impacts and changes in natural ecosystems all demonstrate the continued vulnerability of the United States to extreme drought events.

With the recent occurrence of high impact drought events across the United States and elsewhere around the world, it has become increasingly clear that there is an urgent need to enhance the accuracy and scope of existing drought forecasting systems to assist the development and implementation of drought mitigation plans by vulnerable stakeholders. Indeed, the creation of robust drought early warning systems that can be objectively verified and are capable of providing probabilistic drought forecasts with spatial and temporal resolutions sufficient for users to make informed management decisions is one of the primary goals of the National Integrated Drought Information System (NIDIS). Though drought at its most basic level is simply the manifestation of decreased precipitation relative to the expected climatology, a uniform definition of drought is difficult to construct because its impact varies with location and economic sector. For instance, water resource managers are typically most concerned about long-term drought conditions that decrease the water supply for municipalities, irrigated agriculture, and industry, whereas dryland farmers are susceptible to drought over much shorter time periods. Significant yield losses can occur even in the absence of long-term rainfall deficits if acute moisture stress occurs during a critical stage of crop development (e.g., Rotter and van de Geijn 1999; Saini and Westgate 1999; Ciais et al. 2005; Mittler 2006; Barnabás et al. 2008; Li et al. 2009; Mishra and Cherkauer 2010; Prasad et al. 2011; Swain et al. 2011; Kebede et al. 2012; Pradhan et al. 2012; Hunt et al. 2014). The combined impact of below-normal rainfall, extreme heat, abundant sunshine, and strong winds can rapidly deplete soil moisture owing to higher evapotranspiration (ET) rates, thereby leading to rapid increases in vegetation stress and the development of “flash drought” conditions (Svoboda et al. 2002; Mozny et al. 2012; Otkin et al. 2013). Flash droughts can be especially disruptive owing to their rapid rate of development and thus require drought early warning systems with daily or weekly update cycles (Pozzi et al. 2013) that consider not only rainfall departures, but also other drought indicators, such as ET, vegetation health, and soil moisture.

Various methods have been developed in recent years to generate drought onset and intensification forecasts at regional to global scales. Many studies have employed statistical techniques such as artificial neural networks, stochastic autoregressive models, and Markov chain models to predict future drought conditions (e.g., Loaiciga and Leipnik 1996; Steinemann 2003; Kim et al. 2003;

Mishra and Desai 2005, 2006; Sen and Boken 2005; Barros and Bowden 2008; Hwang and Carbone 2009; Lyon et al. 2012; Özger et al. 2012). Seasonal drought forecasts can also be created using output from sophisticated hydrologic and coupled atmosphere–ocean–land general circulation models (e.g., Wood et al. 2002; Luo et al. 2007; Luo and Wood 2008; Quan et al. 2012; Dutra et al. 2013; Yuan et al. 2013; Yuan and Wood 2013; Bell et al. 2013; Pan et al. 2013; Kirtman et al. 2014). The Climate Prediction Center (CPC) also produces seasonal and monthly Drought Outlook forecast products that identify areas likely to experience changing drought conditions. The CPC products are created each month by propagating the existing drought state, as embodied by the USDM, forward to the next forecasting period using long-range temperature and precipitation forecasts. Though seasonal drought forecasts tend to be closely tied to anomalous circulation patterns associated with the El Niño–Southern Oscillation phenomenon (e.g., Hoerling and Kumar 2003; Schubert et al. 2007), intrinsic atmospheric variability and land surface feedbacks acting over subseasonal time scales are also important (e.g., Kumar et al. 2013; Guo and Dirmeyer 2013). This is especially true in the midlatitudes, where remote forcing due to tropical sea surface temperature anomalies is weaker (Madden 1976; Kumar and Hoerling 1997; Schubert et al. 2004). Indeed, the devastating 2012 flash drought across the central United States resulted primarily from natural variations in weather rather than external forcing due to tropical sea surface temperatures (Hoerling et al. 2014).

Most drought forecasting systems only have monthly update cycles and produce seasonal to annual forecasts more suitable for hydrological applications; therefore, they lack the temporal resolution required to provide early warning of drought development over weekly time scales potentially useful for other stakeholder groups. Given the high economic cost associated with recent drought events, the development of new methods that can be used to provide forecasts over weekly to monthly time scales is imperative. A promising approach is to use rapid changes in satellite-derived drought indices such as the evaporative stress index (ESI) (Anderson et al. 2007c, 2011) to identify areas with an elevated risk for rapid drought development. Case study analyses have shown that rapid decreases in the ESI, which represents standardized anomalies in the ratio of actual to reference ET, often precede periods of rapid drought intensification in the USDM by up to several weeks (Anderson et al. 2013; Otkin et al. 2013). Since anomalous weather patterns conducive to drought development can persist for many weeks, Otkin et al. (2014) developed a new metric known as the rapid change index (RCI) that expresses the cumulative magnitude of the weekly ESI change anomalies

during each rapid change event. Their results showed that drought severity, as classified by the USDM, was more likely to intensify when the RCI was negative, with the highest risk relative to the baseline climatology encompassing the central and eastern United States in areas most susceptible to rapid drought development. For instance, during the 2012 drought, the RCI became strongly negative across a large portion of the central United States more than one month before the USDM drought depiction underwent a rapid deterioration from no drought to extreme drought conditions. This event occurred in the absence of strong external forcing, with little to no warning of its rapid development evident in traditional drought metrics or in climate model simulations (Kumar et al. 2013). These results suggest that the temporal tendency of drought indices may provide useful drought early warning signals that could potentially augment existing drought monitoring and forecasting systems based on prognostic climate and hydrological models.

In this paper, we assess the ability of rapid changes in three drought indices that depict anomalies in ET, precipitation, and soil moisture, respectively, to provide early warning of an elevated risk for drought development across the CONUS during the warm season when vegetation is growing (April–October). RCI variables are constructed in a similar manner for each dataset, with a simple statistical approach used to convert the weekly RCI values into drought intensification probabilities depicting the likelihood that the USDM drought depiction will change during different time periods. Sections 2 and 3 contain descriptions of the various datasets and the methodology used to construct the drought intensification forecasts. Results are shown in section 4, with conclusions provided in section 5.

## 2. Datasets

### a. Evaporative stress index

The ESI represents standardized anomalies in ET fraction ( $ET/F_{ref}$ ), where  $F_{ref}$  is a reference ET flux based on the Penman–Monteith formulation (Allen et al. 1998) that is used to minimize the impact of non-moisture-related drivers on ET, such as the seasonal cycle in solar radiation. Actual ET estimates used to compute the ESI are obtained from the Atmosphere–Land Exchange Inverse (ALEXI) model (Anderson et al. 1997, 2007b). ALEXI is a two-source energy balance model (Norman et al. 1995) that uses remotely sensed land surface temperatures (LSTs) obtained from geostationary satellite thermal infrared (TIR) imagery to compute energy fluxes for bare soil and vegetated components of the land surface. The surface energy budget is inferred using the observed rise in LST from  $\sim 1.5$  h after local sunrise until 1.5 h before local

noon. Closure of the energy balance equations over the morning integration period is obtained using an atmospheric boundary layer (ABL) model developed by McNaughton and Spriggs (1986). Because ALEXI uses the morning rise in LST to compute evapotranspiration, it can only be applied to pixels that remain clear during the morning. Though most cloudy pixels are successfully removed using a cloud mask algorithm, optically thin clouds are more difficult to detect and can lead to spurious ET retrievals if they are not correctly identified. Errors due to incomplete cloud screening are reduced using a temporal smoothing algorithm that identifies days with ET estimates that differ greatly from surrounding times since large differences are likely owing to cloud contamination rather than to abrupt changes in soil moisture content (Anderson et al. 2013). The remaining clear-sky ET estimates are composited over longer multiweek time periods to achieve more complete domain coverage. Daily ET values are typically computed at least once per week for 75% of the grid points, with 95% of the domain updated at least once every 20 days. Though compositing may delay the response time of the ET composites to changing soil moisture conditions, this delay should be minor because droughts are typically associated with clear skies that promote more frequent ET updates (Anderson et al. 2007b).

The ALEXI model is run each day over the CONUS with 10-km horizontal grid spacing using insolation estimates from the Geostationary Operational Environmental Satellite (GOES) imager (Otkin et al. 2005) and hourly LST estimates retrieved from GOES sounder observations. Vegetation cover fraction estimates used to partition the LST and energy fluxes between soil and vegetation components were derived from the Moderate Resolution Imaging Spectroradiometer (MODIS) leaf area index product (MOD15A) (Myneni et al. 2002). Boundary layer temperature lapse rates used by the ABL model were taken from the North American Regional Reanalysis (NARR) (Mesinger et al. 2006). For a complete description of the ALEXI model, the reader is referred to Anderson et al. (2007a).

ESI anomalies, expressed as pseudo  $z$  scores normalized to a mean of 0 and a standard deviation of 1, are computed each week during the nominal growing season (April–October) for 2- and 4-week composite periods. Data from the 2000–13 ALEXI period of record are used to compute the mean ET fraction and standard deviation at each grid point for each composite period. Standardized anomalies are computed as

$$ESI(w, y) = \frac{\langle V(w, y) \rangle - \frac{1}{ny} \sum \langle V(w, y) \rangle}{\sigma(\omega)}, \quad (1)$$

where the first term (within angle brackets) in the numerator is the composite value for week  $w$  and year  $y$  at a given grid point, the second term is the mean condition for week  $w$  averaged over all years, and the denominator is the standard deviation. With this formulation, negative (positive) values indicate lower (higher) soil moisture content and poorer (better) than average vegetation health.

#### *b. Standardized precipitation index*

Accumulated precipitation obtained from the CPC unified analysis of daily precipitation reports from official National Weather Service reporting stations and cooperative observers (Higgins et al. 2000) was used to compute the standardized precipitation index (SPI) (McKee et al. 1993, 1995). The SPI is widely employed to detect meteorological drought conditions and uses precipitation as its sole input. It is a standardized quantity so that values less than zero indicate that the observed precipitation was less than the climatological median precipitation over a given time period. Daily precipitation from 1948 to 2013 was interpolated from the  $0.25^{\circ}$ -resolution grid to the ALEXI model domain using a nearest neighbor approach and was then used to compute 4- and 8-week SPI values at weekly intervals.

#### *c. North American Land Data Assimilation System*

Soil moisture anomalies were computed using data from the North American Land Data Assimilation System (NLDAS) maintained by the National Centers for Environmental Prediction (Xia et al. 2012a,b). Soil moisture content in the top 2 m of the soil profile was obtained from the Noah (Ek et al. 2003; Barlage et al. 2010; Wei et al. 2013), Mosaic (Koster and Suarez 1994, 1996), and Variable Infiltration Capacity (Liang et al. 1996; Bowling and Lettenmaier 2010) models. Though each model simulates surface energy and water balance, and soil moisture in multiple layers, their treatment of infiltration, drainage, vegetation rooting depth, canopy uptake, and soil evaporation differs, which can lead to different responses owing to local climate, soil, and vegetation characteristics. Validation studies have shown that the skill of the models is good in terms of anomaly correlations; however, errors in the simulated soil moisture magnitude can be large for any particular model. Given this variability, the ensemble average was computed since this has been shown to more accurately depict drought conditions (Xia et al. 2014). Soil moisture data from 1979 to 2013 were interpolated from the  $0.125^{\circ}$ -resolution grid to the ALEXI domain using a nearest neighbor approach, with 2- and 4-week standardized total column (0–2 m) soil moisture anomalies (hereafter referred to as NTC) computed at weekly intervals using the ensemble mean.

#### *d. USDM*

The drought intensification probabilities described in section 3 were computed using USDM analyses that classify dryness/drought into five categories ranging from abnormal dryness to exceptional drought (Svoboda et al. 2002). The USDM is created each week through expert synthesis of numerous data streams, including drought diagnostic metrics, surface streamflow, soil moisture, rainfall anomalies, crop and range conditions, and local impact reports from observers across the country. For this study, USDM analyses from the National Drought Mitigation Center were interpolated to the ALEXI domain by assigning numerical values to each drought category, with no drought set to  $-1$ , abnormally dry ( $D0$ ) =  $0$ , moderate drought ( $D1$ ) =  $1$ , severe drought ( $D2$ ) =  $2$ , extreme drought ( $D3$ ) =  $3$ , and exceptional drought ( $D4$ ) =  $4$ .

#### *e. Soil moisture and crop condition data*

The drought intensification probabilities computed with respect to the USDM will also be compared to changes in crop and soil moisture conditions compiled each week by the U.S. Department of Agriculture National Agricultural Statistics Service (NASS) using county-level surveys by local experts. Crop conditions are reported for all major agricultural crops, including corn, soybeans, spring wheat, winter wheat, cotton, peanuts, sorghum, oats, barley, and rice, along with pasture and range conditions. Categorical assessments ranging from very poor to excellent are made for each crop, with the latter indicating the absence of drought stress. For this study, numerical values were assigned to each category (very poor, poor, fair, good, and excellent), with the average condition computed at each grid point using all crop condition reports available during a given week. Categorical topsoil moisture (0–15 cm) assessments ranging from very short to surplus are also available, with the former indicating that soil moisture is significantly less than required for normal plant development. Because of the confidential nature of these datasets, the monthly county-level values were interpolated to the 10-km ALEXI grid and then spatially smoothed using a  $3 \times 3$  pixel square moving window. Though these datasets are qualitative, they still provide a useful independent assessment of drought impacts experienced by agricultural crops.

### 3. Methods

As discussed in the introduction, a recent study by Otkin et al. (2014) has shown that temporal changes in the ESI, as embodied by the RCI, can convey useful information about the rate at which moisture stress is

increasing and can thus provide early warning of an elevated risk for drought development. In this paper, a simple method is used to convert weekly RCI values into probabilistic drought intensification forecasts that are easier to interpret and also incorporate the effects of local climatology. The same methodology is also applied to SPI and NTC anomalies to investigate the

general utility of using temporal changes in drought indices to predict short-term drought development.

#### *a. Rapid change index*

The RCI for a given variable, such as the 4-week ESI composite, is computed using standardized anomalies in the difference between two time periods:

$$\Delta V(w_1, w_2, y) = \frac{V(w_2, y) - V(w_1, y) - \frac{1}{ny} \sum_{y=1}^{ny} [V(w_2, y) - V(w_1, y)]}{\sigma(w_1, w_2)}, \quad (2)$$

where  $w_1$  and  $w_2$  are the weeks used in the difference computation,  $y$  is the year,  $V$  is the variable being differenced, and the denominator is the standard deviation. The RCI can be computed using change anomalies derived from any composite and time differencing combination; however, Otkin et al. (2013) have shown that variables with shorter time periods typically provide earlier warning of drought development because they respond more quickly to changing conditions. Thus, to emphasize fast response times, four RCI variables were computed for each dataset using 1- and 2-week time differencing intervals (denoted CH1 and CH2, respectively) and two short-duration composite periods. For the ESI and NTC datasets, 2- and 4-week anomalies were used, whereas anomalies over longer 4- and 8-week time periods were used for the SPI dataset because the episodic nature of rainfall can introduce large weekly oscillations if shorter time periods are used. In addition, since soil moisture anomalies depicted by the shorter-duration ESI and NTC composites represent the impact of rainfall departures occurring over a longer time period, longer-duration SPI anomalies promote a similar effective response time for all three datasets.

At the beginning of each growing season, nominally defined as 1 March, each RCI variable is set to zero. The RCI then decreases (increases) during subsequent weeks only if the corresponding  $\Delta V$  change anomaly [Eq. (2)] is below (above) a certain threshold. Following Otkin et al. (2014), this threshold was set to  $\pm 0.75$  to highlight areas of unusually large moisture changes. For a given week, the RCI is computed as

$$RCI = RCI_{prev} - \sqrt{\text{abs}(\Delta V) - 0.75} \quad \text{if } \Delta V < -0.75; \quad (3)$$

$$RCI = RCI_{prev} + \sqrt{\Delta V - 0.75} \quad \text{if } \Delta V > 0.75, \quad (4)$$

where  $RCI_{prev}$  is the RCI value from the previous week. The RCI will reset to zero if the sign of the  $\Delta V$  anomaly

is opposite that of the prior week, but it will remain unchanged if the  $\Delta V$  anomaly has the same sign as the prior week but is less than the threshold value. The RCI is not reset to zero in these situations to help prevent the separation of long-duration rapid change events into multiple shorter events. With this formulation, negative (positive) RCI values correspond to periods of rapidly increasing (decreasing) moisture stress.

Values for the full suite of 12 RCI variables (two composite and two change intervals for each of the three drought indices) were computed each week during 2000–13. Because each variable responds differently to changing conditions, a limited number of sensitivity tests were then performed to identify suitable weights with which to combine the four RCI variables computed for each drought index into a single RCI value, hereafter referred to as  $RCI_{ESI}$ ,  $RCI_{NTC}$ , and  $RCI_{SPI}$ . These tests, which consisted of a qualitative analysis of drought events across the central and eastern United States, showed that a weighted average emphasizing the shorter differencing and composite periods provided good drought early warning signals, such that

$$RCI_{ESI} = 0.6 \times CH1\_02WK + 0.3 \times CH1\_04WK + 0.1 \times CH2\_02WK, \quad (5)$$

$$RCI_{NTC} = 0.6 \times CH1\_02WK + 0.3 \times CH1\_04WK + 0.1 \times CH2\_02WK, \quad \text{and} \quad (6)$$

$$RCI_{SPI} = 0.6 \times CH1\_04WK + 0.3 \times CH1\_08WK + 0.1 \times CH2\_04WK. \quad (7)$$

While a detailed analysis of optimal forms for these equations is beyond the scope of the current study, future work will investigate further refinements to optimize performance.

### *b. Drought intensification probabilities*

After computing average RCI values for each drought index, a simple method was used to convert the weekly RCI values into drought intensification probabilities at each grid point. Ten years (2000–09) of RCI data are used as a training period to compute the necessary parameters, with the following four years (2010–13) used to validate the method. First, for each week during the training period with a negative RCI value, the maximum increase in USDM drought severity was computed for subsequent 2-, 4-, and 8-week time periods. The negative RCI values were then separated into one-unit bins ranging from 0 to –10, with the complete sample for each forecast lead time used to compute the probability that the USDM drought depiction will worsen by at least one, two, or three categories for RCI values in each bin. A linear least squares line was then fit through the computed probabilities to determine the *y* intercept and slope for each forecast and intensification combination for each drought index. These parameters were then used to convert the weekly RCI values into drought intensification probabilities during the training and validation periods. Because the slope and intercept values are computed at each grid point, this method accounts for the local climatology by potentially converting the same RCI value into different intensification probabilities for different parts of the United States. Thus, the probabilities may contain more useful information than the unconverted RCI values.

## 4. Results

### *a. Regional drought case study*

In this section, the spatial and temporal congruence between the RCI and RCI-derived drought intensification probabilities and changes in the corresponding USDM and NASS datasets is examined for a rapid onset drought event that occurred across the central United States during the training period. Figure 1 shows the evolution of the USDM, NASS, and RCI datasets at 2-week intervals from 3 June to 12 August 2002, with the corresponding drought intensification probabilities shown in Fig. 2. At the beginning of June, moderate to extreme drought conditions (D1–D3) were present across the central high plains with abnormally dry conditions (D0) extending farther to the north. By this time, large RCI values and drought intensification probabilities had developed across South Dakota and Minnesota in response to a prolonged period of dry weather. The topsoil moisture and crop health status subsequently deteriorated across South Dakota as severe drought expanded northward; however, heavy rainfall farther east prevented drought emergence over Minnesota.

By the beginning of July, very hot temperatures and below-normal rainfall led to rapidly increasing moisture stress along the northeastern periphery of the core drought region, with a wide band of negative RCI\_ESI values developing from western South Dakota to eastern Kansas. Except for a large gap in central Nebraska where change anomalies were negative but did not exceed the –0.75 threshold, the RCI\_SPI and RCI\_NTC datasets also indicate that conditions were deteriorating across the region. The drought intensification probabilities (Fig. 2) showed that many locations had at least a 20% chance that the USDM drought analysis would deteriorate by at least two categories during an 8-week period, which is much higher than the average probability based on the 2000–12 climatology (Otkin et al. 2014). Indeed, conditions rapidly worsened during the next few weeks, with an extensive area experiencing at least a two-category increase in drought severity. Though the NASS topsoil moisture anomalies remained relatively constant during this time period, very large crop condition anomalies developed across the region by the middle of August (Fig. 1). Drought continued to expand southeastward into eastern Kansas and western Missouri during late summer (not shown) within the region of high intensification probabilities at the end of July. This example presents evidence that unusually rapid changes in the ESI, SPI, and NTC datasets can provide early warning of drought development in the USDM that is consistent with observed changes in the NASS crop condition and soil moisture datasets.

### *b. Local drought case studies: Training period*

This section examines the evolution of two drought events that occurred during the statistical training period through a comparison of drought indicators, meteorological data, crop conditions, and RCI-derived drought intensification probabilities. To more easily display the wealth of information provided by these variables, a new visualization method was developed. Figure 3 shows the evolution of the USDM, weekly rainfall, NARR surface temperature anomalies, NASS topsoil moisture and crop conditions, and ESI, SPI, and NTC anomalies, along with each of the RCI variables and their associated drought intensification probabilities, averaged over all grid points in the “Rolling Plains of Texas” (CPC climate division 2) during 2003. This region contains a mixture of range and farmland, with wheat, sorghum, cotton, and forage being the dominant crops.

Though weather conditions during April were cooler than normal, negative ESI, SPI, and NTC anomalies indicate that moisture stress remained elevated across the region owing to a lack of heavy rainfall. Drought intensification probabilities computed using the RCI\_ESI

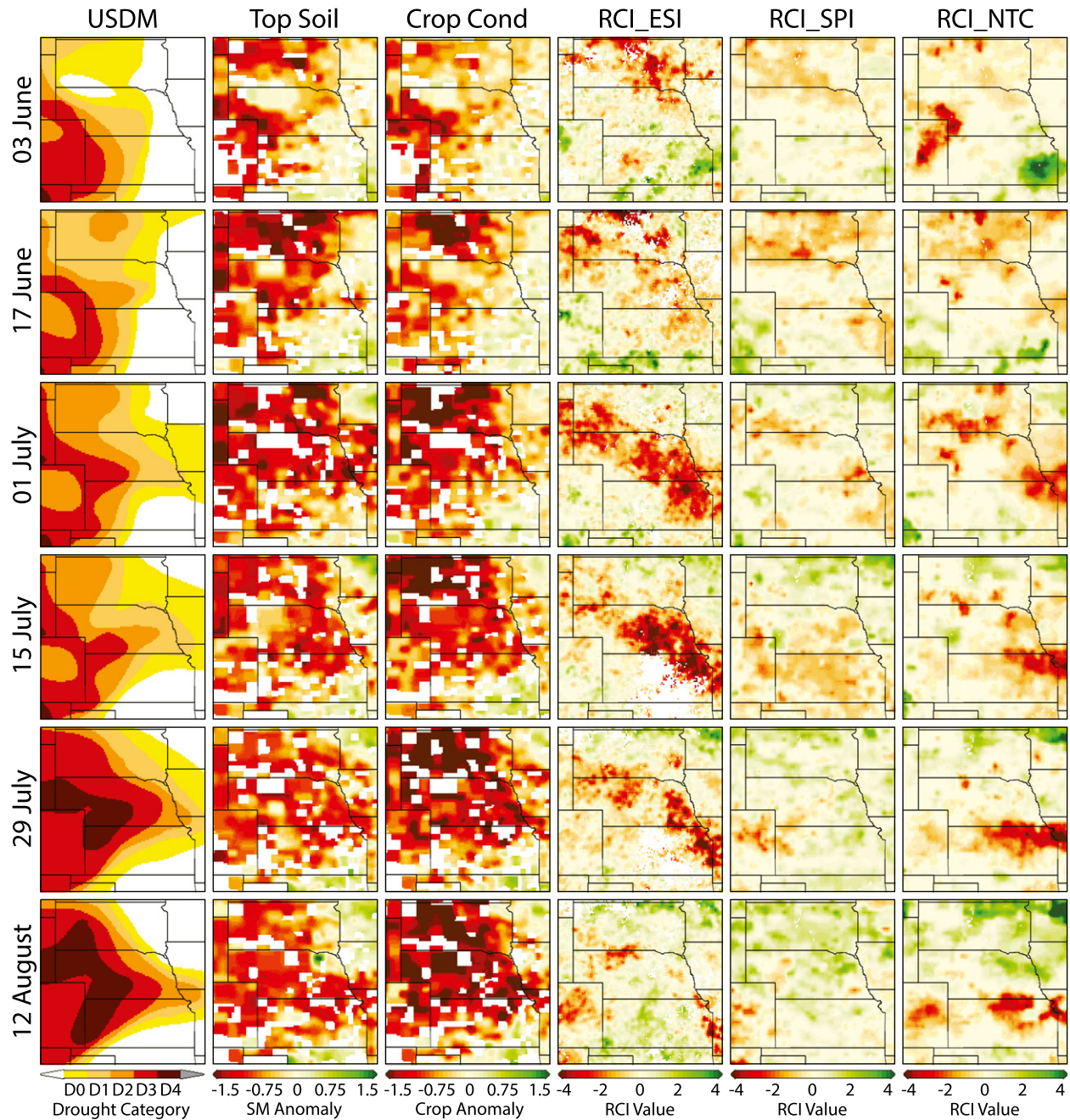


FIG. 1. Temporal evolution of USDM drought depiction, NASS topsoil moisture anomaly, NASS crop condition anomaly, RCI\_ESI, RCI\_SPI, and RCI\_NTC from 3 Jun to 12 Aug 2002.

and RCI\_NTC datasets indicated a high probability that drought would worsen during the next few weeks. These probabilities were much higher than those derived from the RCI\_SPI dataset because light rain events throughout the month prevented a more rapid decrease in the SPI. Moderate drought conditions subsequently developed at the beginning of May and persisted for several weeks before a prolonged period of cool, wet weather

eliminated drought conditions by the beginning of July. All variables indicated favorable conditions during June, with intensification probabilities at or near zero. Very dry weather returned to the area by the middle of July, however, with temperatures at or above normal. The less favorable conditions led to rapid decreases in the ESI, SPI, and NTC anomalies and to the rapid appearance of large intensification probabilities during the first half of

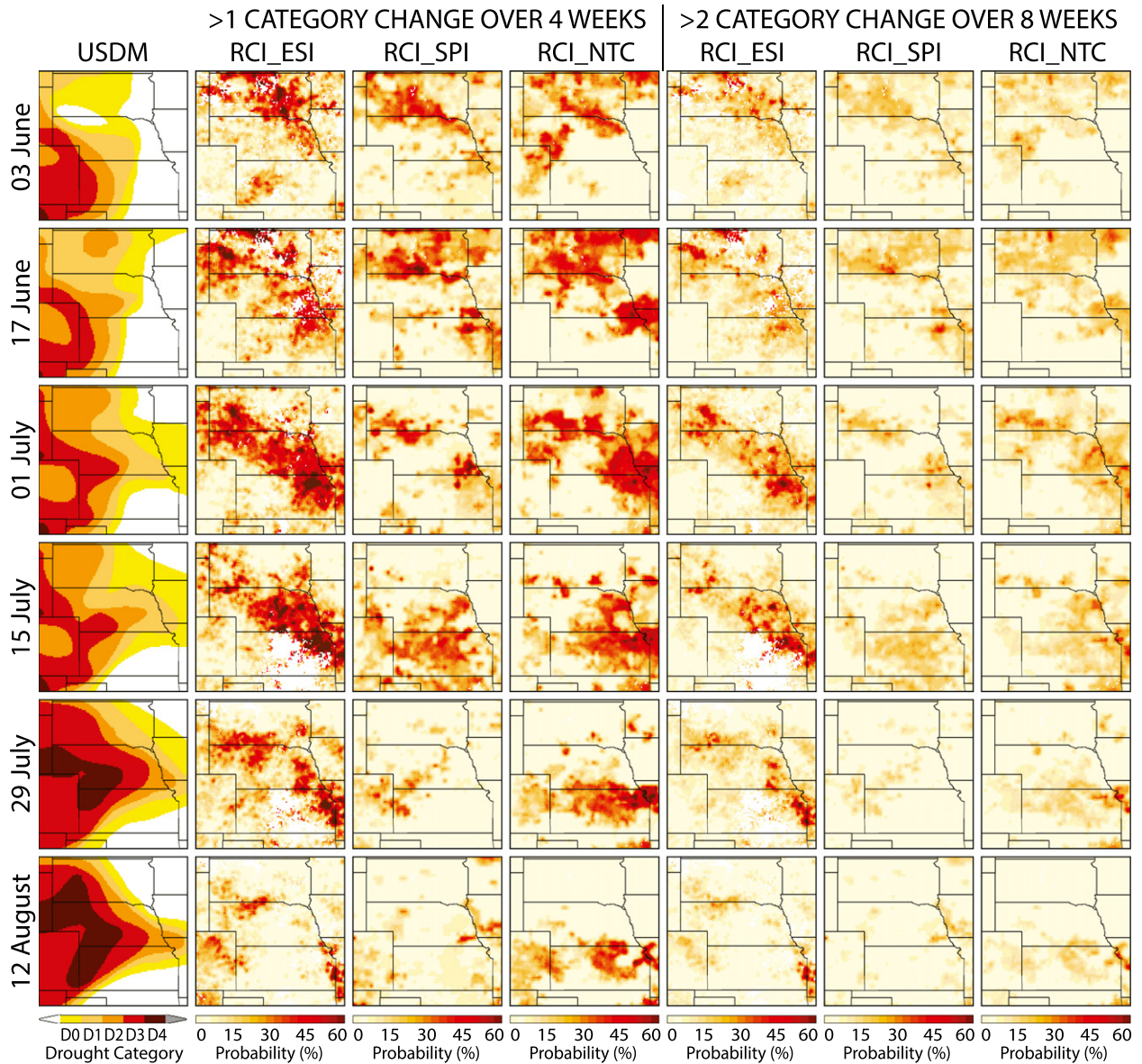


FIG. 2. Temporal evolution of the USDM drought depiction from 3 Jun to 12 Aug 2002 (first column). The probability of at least a one-category increase in the USDM drought depiction over a 4-week period computed using the RCI\_ESI, RCI\_SPI, and RCI\_NTC variables is shown in columns 2–4, with columns 5–7 showing the probability of at least a two-category increase occurring over an 8-week period.

July, even though the underlying indices remained positive. The initial appearance of the high probabilities occurred at the same time as the reintroduction of abnormal dryness in the USDM but occurred several weeks prior to the rapid transition from abnormal dryness to severe drought during August. The enhanced risk for drought development indicated by the RCI variables at the beginning of July also preceded a rapid deterioration in the soil moisture and crop condition datasets.

Figure 4 depicts the evolution of a slower-developing drought event that occurred within an intensively managed

agricultural landscape across east-central Nebraska during the summer of 2006. Severe drought conditions were present across the region during late winter (not shown); however, heavy rainfall during the spring led to more favorable conditions, as evidenced by the mostly positive SPI and NTC anomalies during April. Drier weather returned during May, with rapid decreases in the SPI and NTC datasets resulting in large drought intensification probabilities. The ESI-derived probabilities were much lower because the ESI exhibited less recovery during the spring, thereby leading to smaller weekly changes during May and smaller RCI values. The RCI\_ESI

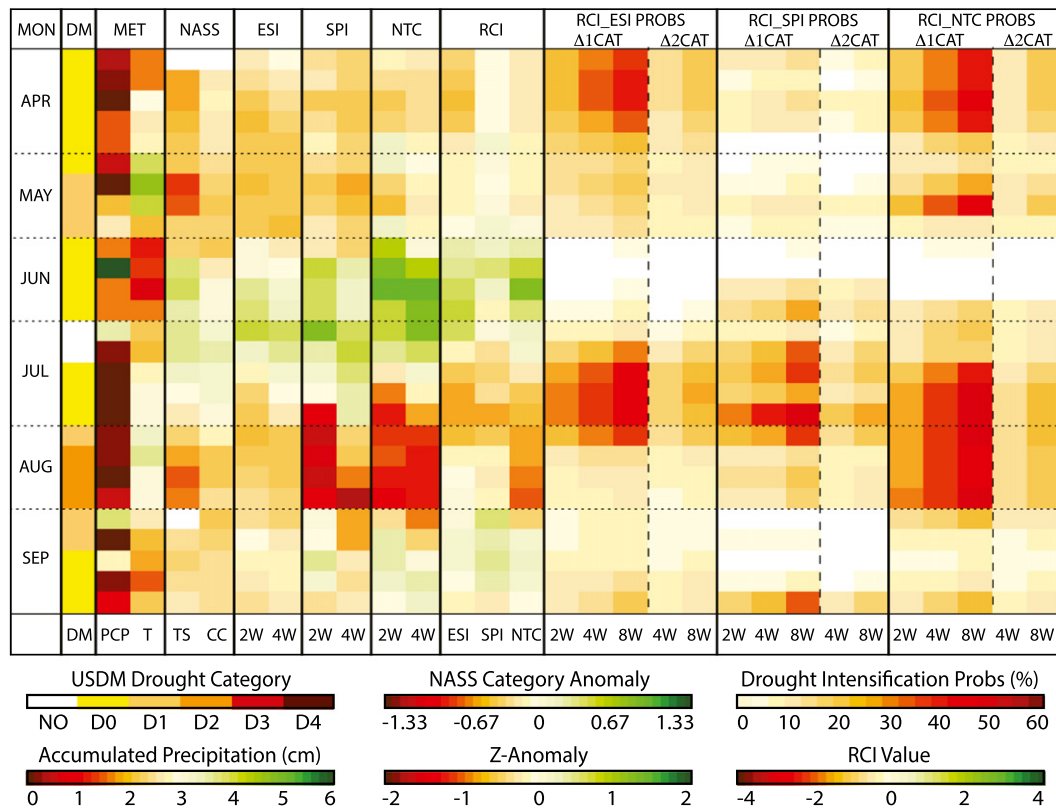


FIG. 3. Drought evolution across the Rolling Plains of Texas (CPC division 2) during 2003. The weekly USDM drought category is shown in column 1, with 1-week rainfall (cm) in column 2, 2-week surface temperature (K) z anomalies in column 3, and NASS topsoil and crop condition anomalies in columns 4 and 5. ESI z anomalies for 2- and 4-week composite periods are shown in columns 6 and 7, with 4- and 8-week SPI and 2- and 4-week NTC z anomalies shown in columns 8 and 9 and 10 and 11, respectively. RCI\_ESI, RCI\_SPI, and RCI\_NTC values are shown in columns 12–14. One-category USDM drought intensification probabilities for 2-, 4-, and 8-week time periods and two-category probabilities for 4- and 8-week periods computed using RCI\_ESI, RCI\_SPI, and RCI\_NTC data are shown in columns 15–19, 20–24, and 25–29, respectively.

and associated probabilities began to increase more rapidly during the latter part of May when much warmer temperatures enveloped the region because the combination of hot temperatures and dry weather can quickly deplete soil moisture reserves (Otkin et al. 2013). A continuation of generally warm and dry weather during the summer caused conditions to steadily deteriorate, with abnormal dryness introduced in the USDM during the second week of June before transitioning to moderate drought at the beginning of July and severe drought several weeks later. Heavy rainfall during August began to erode the drought conditions and led to intensification probabilities at or near zero for the rest of the growing season.

#### c. Local drought case studies: Validation period

To further assess the ability of the drought intensification probabilities to provide useful drought early warning signals, this section examines the evolution of two

drought events that occurred during the validation period. The first event (Fig. 5) occurred across east-central Oklahoma during 2011 within a region characterized by a mixed landscape of pasture, range, and forest. Moderate drought conditions were present across the region at the beginning of the growing season owing to below-normal winter precipitation; however, very heavy rainfall during April and May eliminated drought conditions according to the USDM and led to a rapid transition to strongly positive 4- and 8-week SPI anomalies. Though the NTC and ESI anomalies also improved during this time period, their recovery was less impressive than what may have been expected based on the SPI because the soil was unable to absorb a large portion of the rainfall owing to very high rainfall rates, thereby limiting soil moisture recharge and vegetation recovery. By the beginning of June, the wetter and cooler-than-normal weather pattern underwent a rapid transition to very hot and dry conditions that persisted throughout the rest of

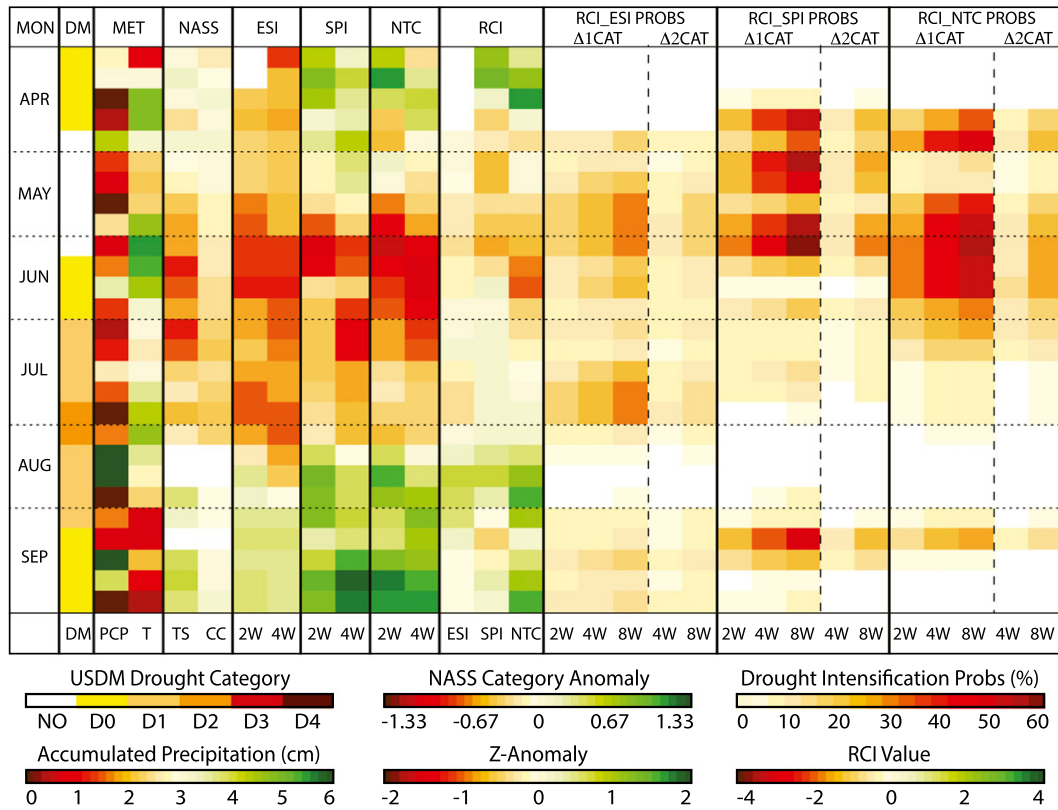


FIG. 4. As in Fig. 3, but for drought evolution across east-central Nebraska (CPC division 6) during 2006.

the summer. Drought rapidly developed across the region, with the USDM drought analysis degrading by one category for three consecutive weeks before stabilizing at an extreme drought (D3) severity level only six weeks after the area was drought free. The NASS topsoil moisture assessment also transitioned from normal conditions to a severe moisture deficit during this time period. Each of the RCI variables became negative by the second week of June, with elevated intensification probabilities thereafter. For this event, rapid changes in the ESI provided the earliest sustained warning of an enhanced risk for drought development. Drought probabilities computed using changes in the NTC dataset provided slightly earlier warning, but were more variable with time. Using a longer anomaly period would help remove some of the weekly variability but would also delay the response time to changing conditions.

The final drought event examined in this section affected south-central Wisconsin during the summer of 2012 (Fig. 6). Record warm temperatures during March combined with below-normal precipitation during the preceding winter resulted in large negative NTC anomalies during April. The unusually warm weather, however, also promoted much earlier vegetation emergence and

growth across the region and thus led to large positive ESI anomalies due to enhanced ET rates. After receiving near-normal rainfall during April and the first half of May, which helped recharge topsoil moisture content, a prolonged period of extremely hot and dry weather during the next two months (June–July) led to a very rapid increase in moisture-related stress. ESI and NTC anomalies rapidly became strongly negative by the middle of May, with the SPI anomalies undergoing a similar transition several weeks later. Very high drought intensification probabilities occurred in the ESI-derived dataset several weeks before the NASS soil moisture and crop condition datasets rapidly deteriorated and up to two months before an unprecedented deterioration of one USDM category per week for four consecutive weeks started at the end of June. The NTC-derived probabilities were also very high, but their initial appearance was later. Compared to the ESI and NTC datasets, weekly changes in the SPI were much smaller, which greatly limited the intensification probabilities computed using the RCI\_SPI data. These results suggest that a greater reliance on drought indices depicting anomalies in soil moisture and vegetation during the USDM mapping process may promote an earlier drought onset depiction, especially for flash

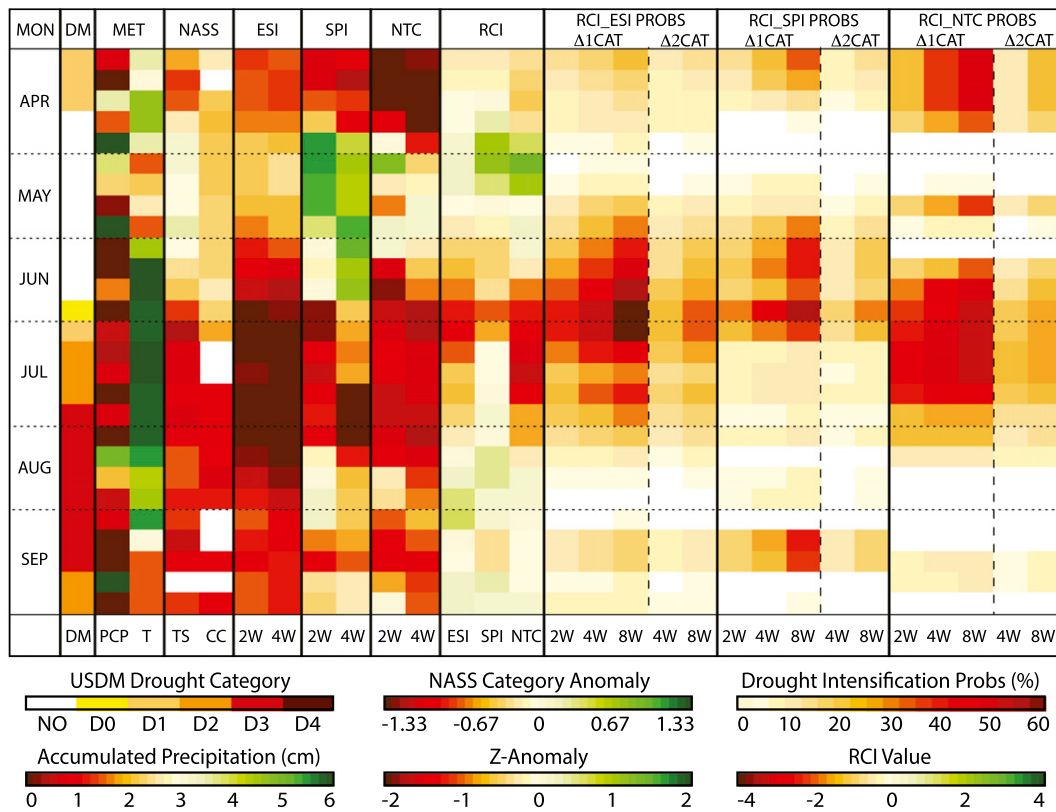


FIG. 5. As in Fig. 3, but for drought evolution across east-central Oklahoma (CPC division 6) during 2011.

drought events that are driven by more than just rainfall departures.

#### *d. Statistical analysis*

The accuracy of the drought intensification probabilities is further assessed in this section using data from the independent 4-yr validation period (2010–13). Figure 7 shows reliability diagrams for RCI predictions of one-category USDM changes occurring over 2-, 4-, and 8-week periods, two-category changes over 4- and 8-week periods, and three-category changes over 8-week periods, computed separately for the western and eastern United States. Reliability diagrams depict how often a forecasted event occurs relative to the predicted likelihood of that event and can be used to assess the forecast confidence. Perfect reliability is achieved when the predicted and actual probabilities are identical, with the values lying along the diagonal line in the reliability diagram.

Overall, the results indicate that the probabilistic forecasts are most reliable over the eastern United States for all intensity change and forecast lead-time combinations, with very low reliability over the western United States. The low reliability in this region may be due to the conservative nature of the USDM, which will cause forecasts based on

rapid changes in drought indices to be overconfident since the USDM analyses in the western United States tend to change only when dry conditions have persisted for a long period of time. This tendency of the USDM to depict long-term drought conditions in the western United States will reduce the reliability of the RCI-derived probabilities since they are sensitive to moisture stress changes occurring over shorter time periods. A detailed comparison of the RCI datasets shows that the ESI-derived probabilities are generally the most reliable, with the best forecasts occurring for one-category USDM changes over all forecast lead times and for two-category changes over an 8-week period. Except for where the climatological probability exceeds the predicted probability, such as the left side of Fig. 7c, the forecast probabilities are too confident, with most points located below the diagonal line. The observed probabilities, however, are usually higher than climatology, which provides evidence that drought development is often preceded by rapid changes in these drought indices. The overconfidence may be due to sampling differences in the training and validation datasets since two of the most intense droughts occurred during the validation period (e.g., 2011 and 2012). Inclusion of these recent drought events in the training dataset may improve future drought forecasts.

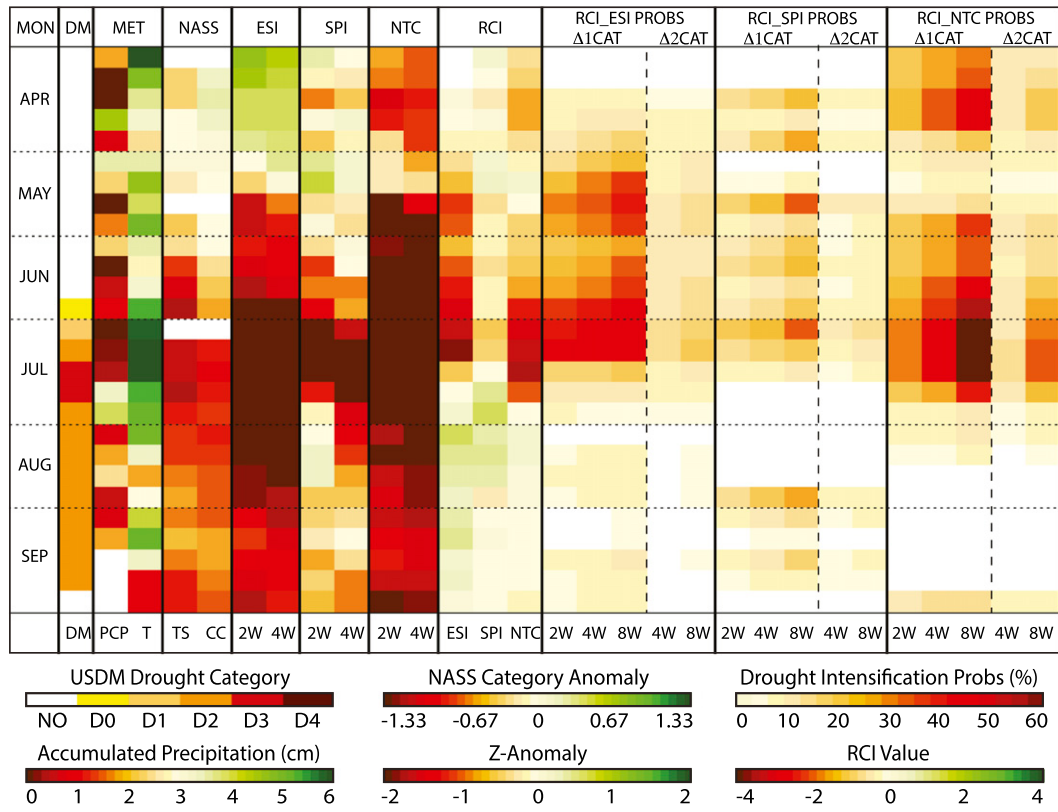


FIG. 6. As in Fig. 3, but for drought evolution across south-central Wisconsin (CPC division 8) during 2012.

Figure 8 shows Brier skill scores for one-category USDM changes occurring over 2-, 4-, and 8-week periods, two-category changes over 4- and 8-week periods, and three-category changes over 8-week periods, computed at each grid point using data from the 2010–13 validation period. Brier skill scores greater than zero indicate that the forecast skill is greater than that achieved using a reference forecast based on climatology (Wilks 2011). For one-category changes, the forecast skill is generally small for shorter lead times but increases greatly for 8-week forecast periods. The lower skill for shorter lead times is due to the tendency for these forecasts to be overconfident (refer to Fig. 7), thereby leading to a higher false alarm rate. For larger two- and three-category changes in the USDM, there is no forecast skill over the western United States; however, some skill is evident across the central United States within areas most susceptible to flash drought development (Otkin et al. 2014). Comparison of the RCI datasets shows that the forecast skill is higher for probabilities derived from changes in the SPI and NTC datasets, which may be due to their previous inclusion in the USDM mapping process. Differences in the spatial patterns of the skill scores also suggest that some combination of the RCI datasets may provide the most skillful drought forecasts.

#### e. Comparison to NASS soil moisture and crop condition datasets

In this section, the ability of rapid changes in the ESI, SPI, and NTC datasets, as encapsulated by the RCI, to provide early warning of deteriorating conditions is further assessed through a correlation analysis with the NASS soil moisture and crop condition datasets. Figure 9 shows the correlation between the maximum RCI value for a given rapid change event and the maximum decrease in the categorical topsoil moisture and crop condition status from the beginning of an event (defined as the first week with a negative RCI value) until two weeks after its conclusion. The correlations were computed separately for each grid point and RCI variable using data from 2002 to 2012.

Overall, correlations between the RCI variables and changes in soil moisture and crop condition status are highest ( $>0.35$ ) across agricultural areas in the central and eastern United States that contain a dense observing network and widespread nonirrigated farmland. For topsoil moisture (Figs. 9a–c), the highest correlations were obtained when using the RCI\_NTC dataset, which is not surprising given that this dataset depicts soil moisture. The correlations were slightly weaker for the ESI and SPI

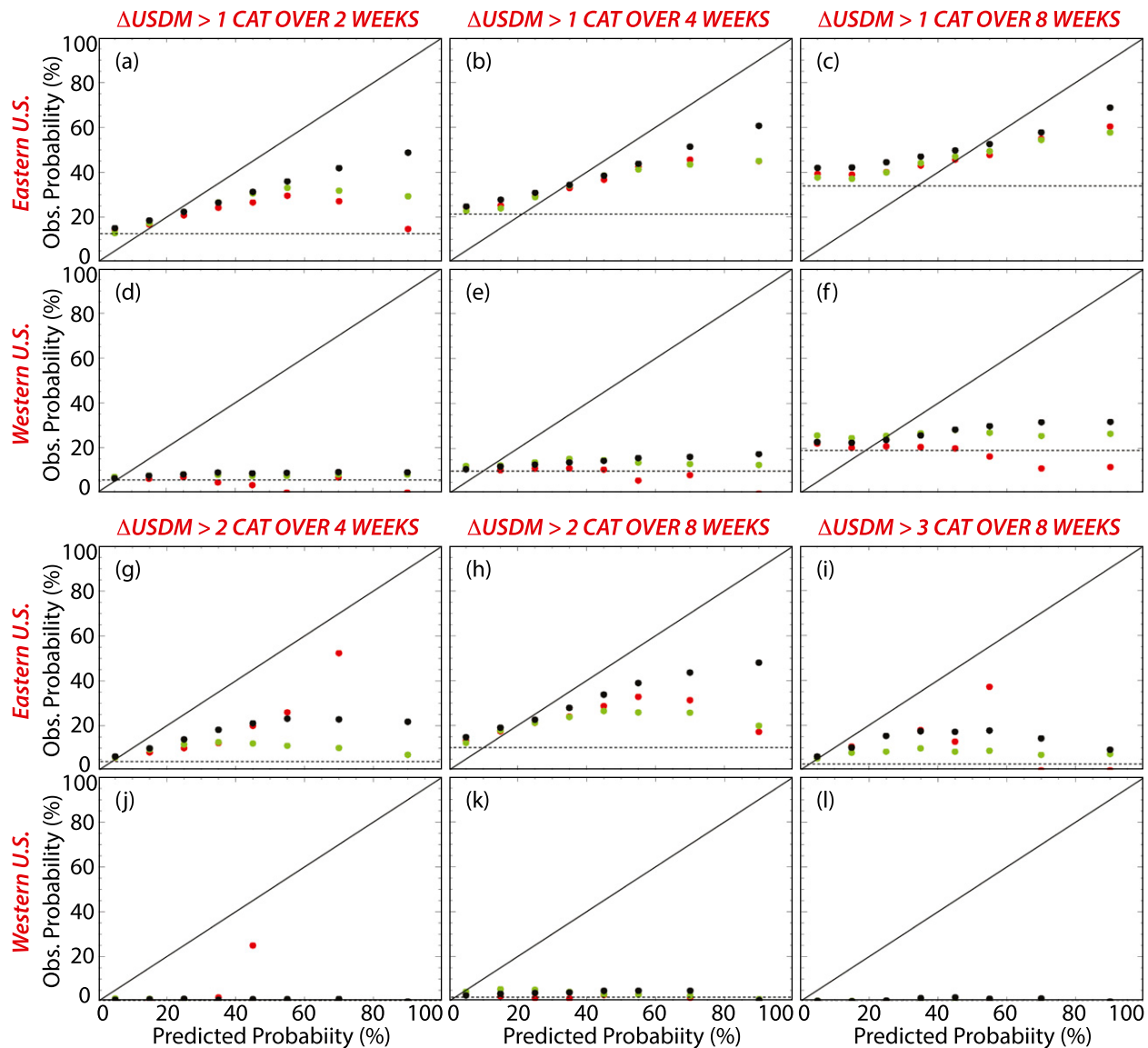


FIG. 7. Reliability diagrams for the drought intensification probabilities computed using the RCI\_ESI (black circle), RCI\_SPI (red circle), and RCI\_NTC (green circle) datasets over the western and eastern United States. Diagrams are shown for one-, two-, and three-category USDM increases over 2-, 4-, and 8-week periods.

datasets; however, the positive correlations still indicate that a relationship exists between rapid changes in these datasets and subsequent decreases in the soil moisture status. For crop conditions (Figs. 9d–f), weaker correlations ( $>0.25$ ) occurred for each RCI dataset, with the largest decreases relative to the soil moisture correlations occurring for the NTC and SPI datasets. The lower correlations may indicate reduced sensitivity of the RCI to changes in crop health status; however, it is also possible that the weaker correlations are simply due to the lag time between increasing soil moisture deficits and observed changes in crop health (e.g., columns 2 and 3 in Figs. 3–6). Vegetation can appear healthy to human

observers even as the moisture stress increases because drought signals often become apparent only after significant damage has already occurred to the plants. This may lower the correlations because there is more time for heavy rainfall to prevent large deteriorations in crop health even if soil moisture deficits are increasing. A new version of the ESI, developed at 4-km resolution using LST retrievals from the GOES Imager, appears to have improved sensitivity to moisture conditions across the western United States in comparison with the 10-km sounder-based ESI dataset evaluated during this study. These spatial analyses will be reevaluated with the new 4-km product in future studies.

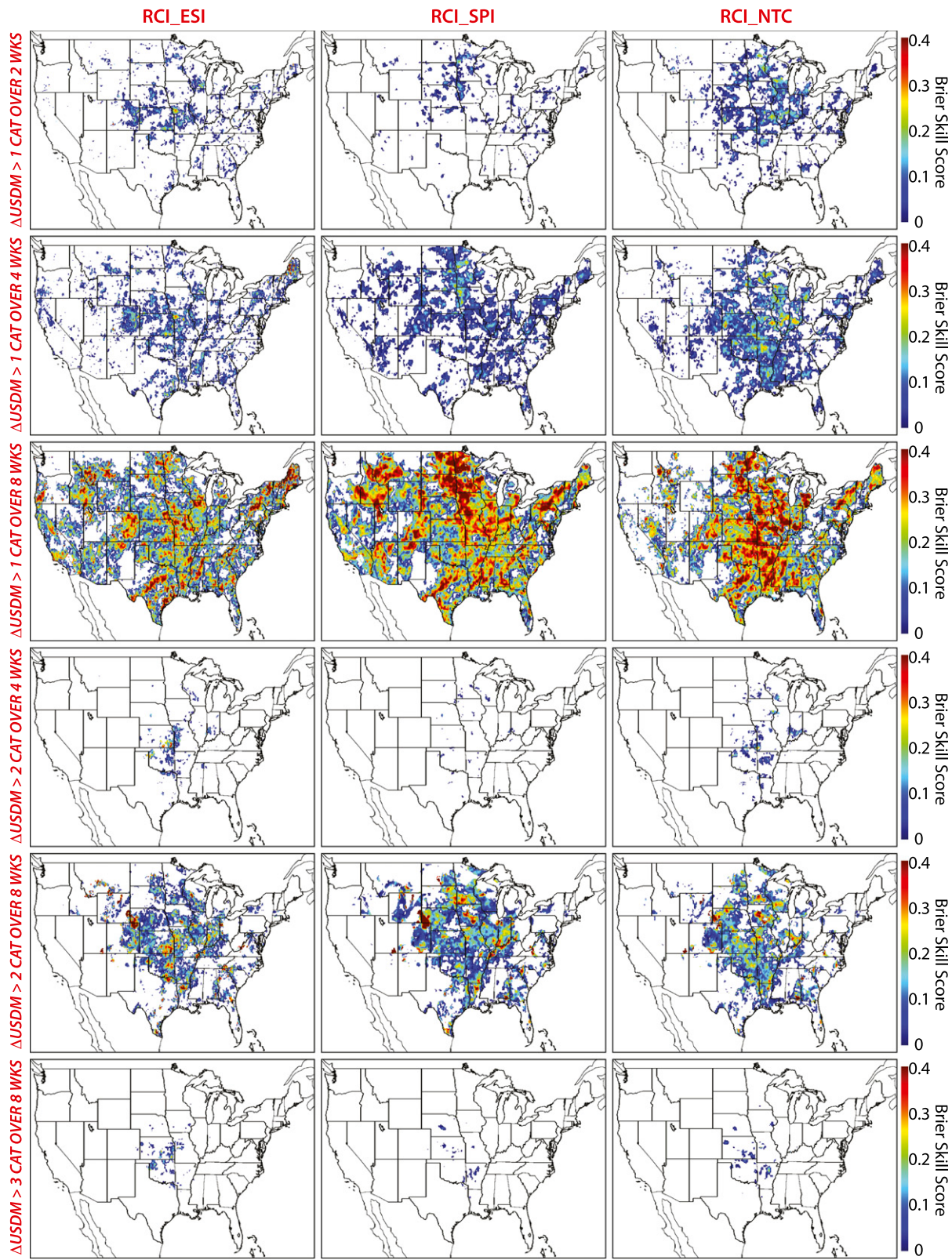


FIG. 8. Brier skill scores computed using drought intensification probabilities derived from the RCI\_ESI, RCI\_SPI, and RCI\_NTC datasets. Images are shown for one-, two-, and three-category USDM increases over 2-, 4-, and 8-week periods.

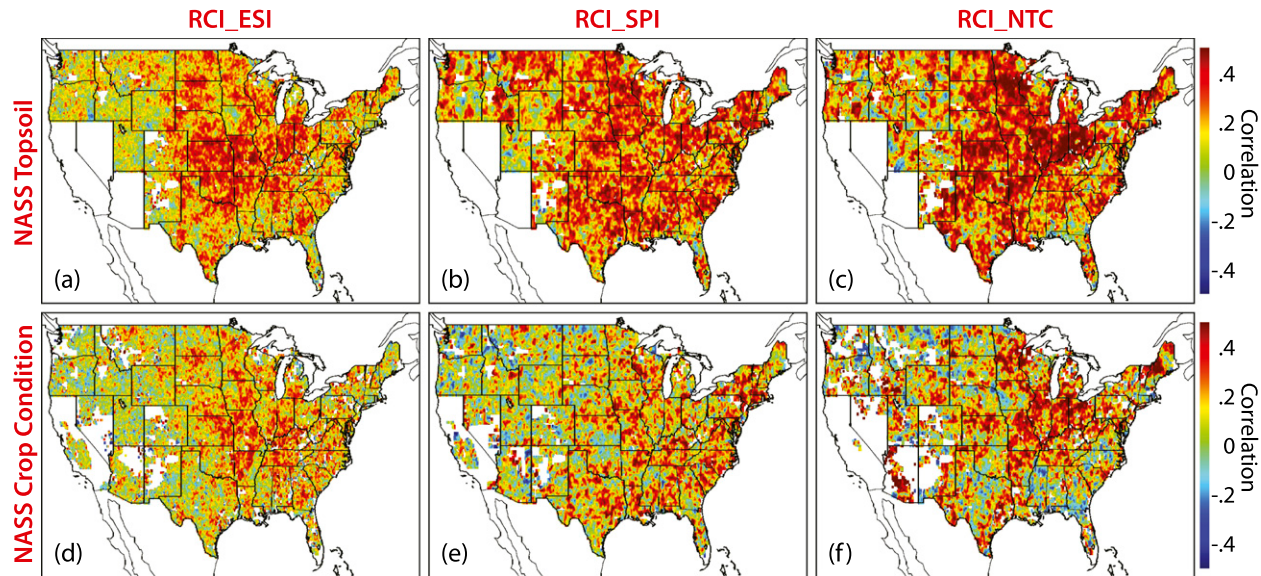


FIG. 9. Correlation between the maximum RCI value for each rapid change event and the maximum decrease in the NASS topsoil moisture classification from the beginning of an event until two weeks after its end for the (a) RCI\_ESI, (b) RCI\_SPI, and (c) RCI\_NTC variables. (d)–(f) As in (a)–(c), but for the correlation between the maximum RCI value for each rapid change event and the maximum decrease in the NASS crop condition classification.

## 5. Conclusions and discussion

This study examined the potential utility of using rapid changes in drought indices depicting anomalies in evapotranspiration, precipitation, and soil moisture to provide early warning of an increased risk for drought development across the CONUS for subseasonal forecast lead times. Standardized change anomalies were computed each week during the 2000–13 growing seasons using ESI, SPI, and NTC anomalies. A new RCI metric first described by Otkin et al. (2014) was then used to encapsulate the accumulated magnitude of rapid changes in these variables, defined as standardized change anomalies greater than  $\pm 0.75$ , during a given rapid change event. After computing the RCI for each drought index, a simple linear least squares statistical method was used to convert the weekly RCI values into drought intensification probabilities depicting the likelihood that the USDM drought depiction would deteriorate by at least one, two, or three categories during subsequent weeks.

Overall, the results revealed that unusually rapid changes in the ESI, SPI, and NTC datasets often precede periods of drought intensification in the USDM and therefore may provide effective early warning of an increased risk for drought development that could potentially be a useful component of future drought early warning systems. Local case study analyses showed that very high RCI-derived intensification probabilities, often several times higher than the background climatology, frequently occurred several weeks prior to changes in the

USDM. Statistical analyses showed that the ESI-derived intensification probabilities were most reliable, especially across the eastern two-thirds of the United States, whereas the SPI and NTC-derived datasets had the highest skill scores, possibly owing to their prior inclusion in the USDM mapping process. Correlation analyses showed that there is also a strong relationship between rapid changes in the drought indices and subsequent deteriorations in the NASS soil moisture and crop condition datasets. Given that these datasets were not used to compute the drought intensification probabilities, the positive correlations provide additional evidence that the RCI variables contain useful drought early warning signals.

Though this study provides a preliminary proof of concept that rapid changes in drought indices can be used to identify areas susceptible to drought development and to produce probabilistic drought intensification forecasts over subseasonal time scales, it should not be viewed as the final answer because many additional studies are necessary to optimize and refine these results. For instance, sensitivity studies are necessary to explore whether using different change anomaly threshold values [e.g., Eqs. (3) and (4)] and variable combinations [e.g., Eqs. (5)–(7)] when computing the RCI can improve forecast skill. Using a longer time period to compute the anomalies may result in a smoother drought early warning signal by reducing the large variability that short-term anomalies can exhibit; however, this may also result in a delayed signal since longer term variables tend to respond more slowly to rapidly changing conditions (e.g., Otkin et al. 2013). One

potential approach would be to generalize the method so that change variables computed using different compositing and differencing intervals are used to create an average RCI at each grid point rather than being applied uniformly across the entire domain, as is done in this study. This may be optimal since the vegetation response to drying conditions may depend on the location and vegetation type. In addition, the statistical method used to convert the weekly RCI values to drought intensification probabilities is very simple. More advanced methods should be explored. Finally, a blended approach that combines information from multiple drought metrics may enhance the robustness and accuracy of the RCI-derived intensification probabilities by providing additional data masks that together provide a more complete depiction of the current drought status. Differences in regional forecast skill and correlations shown during this study support this possibility.

**Acknowledgments.** This work was supported by funds provided by the NOAA Climate Program Office's Sectoral Applications Research Program (SARP) and the Modeling, Analysis, Predictions, and Projections (MAPP) program under Grants NA13OAR4310122 and GC09-236.

## REFERENCES

- Allen, R. G., L. S. Pereira, D. Raes, and M. Smith, 1998: Crop evapotranspiration: Guidelines for computing crop water requirements. FAO Irrigation and Drainage Paper 56, 300 pp. [Available online at [www.fao.org/docrep/X0490E/X0490E00.htm](http://www.fao.org/docrep/X0490E/X0490E00.htm).]
- Anderson, M. C., J. M. Norman, G. R. Diak, W. P. Kustas, and J. R. Mecikalski, 1997: A two-source time-integrated model for estimating surface fluxes using thermal infrared remote sensing. *Remote Sens. Environ.*, **60**, 195–216, doi:[10.1016/S0034-4257\(96\)00215-5](https://doi.org/10.1016/S0034-4257(96)00215-5).
- , W. P. Kustas, and J. M. Norman, 2007a: Upscaling flux observations from local to continental scales using thermal remote sensing. *Agron. J.*, **99**, 240–254, doi:[10.2134/agronj2005.0096S](https://doi.org/10.2134/agronj2005.0096S).
- , J. M. Norman, J. R. Mecikalski, J. A. Otkin, and W. P. Kustas, 2007b: A climatological study of evapotranspiration and moisture stress across the continental U.S. based on thermal remote sensing: 1. Model formulation. *J. Geophys. Res.*, **112**, D10117, doi:[10.1029/2006JD007506](https://doi.org/10.1029/2006JD007506).
- , —, —, —, and —, 2007c: A climatological study of evapotranspiration and moisture stress across the continental U.S. based on thermal remote sensing: 2. Surface moisture climatology. *J. Geophys. Res.*, **112**, D11112, doi:[10.1029/2006JD007507](https://doi.org/10.1029/2006JD007507).
- , C. Hain, B. Wardlow, A. Pimstein, J. R. Mecikalski, and W. P. Kustas, 2011: Evaluation of drought indices based on thermal remote sensing and evapotranspiration over the continental United States. *J. Climate*, **24**, 2025–2044, doi:[10.1175/2010JCLI3812.1](https://doi.org/10.1175/2010JCLI3812.1).
- , —, J. A. Otkin, X. Zhan, K. Mo, M. Svoboda, B. Wardlow, and A. Pimstein, 2013: An intercomparison of drought indicators based on thermal remote sensing and NLDAS simulations. *J. Hydrometeor.*, **14**, 1035–1056, doi:[10.1175/JHM-D-12-0140.1](https://doi.org/10.1175/JHM-D-12-0140.1).
- Aon Benfield, 2013: Annual global climate and catastrophe report: Impact forecasting—2012. Impact Forecasting Rep., 96 pp. [Available online at [http://thoughtleadership.aonbenfield.com/Documents/20130124\\_if\\_annual\\_global\\_climate\\_catastrophe\\_report.pdf](http://thoughtleadership.aonbenfield.com/Documents/20130124_if_annual_global_climate_catastrophe_report.pdf).]
- Barlage, M., and Coauthors, 2010: Noah land surface model modifications to improve snowpack prediction in the Colorado Rocky Mountains. *J. Geophys. Res.*, **115**, D22101, doi:[10.1029/2009JD013470](https://doi.org/10.1029/2009JD013470).
- Barnabás, B., K. Jäger, and A. Fehér, 2008: The effect of drought and heat stress on reproductive processes in cereals. *Plant Cell Environ.*, **31**, 11–38, doi:[10.1111/j.1365-3040.2007.01727.x](https://doi.org/10.1111/j.1365-3040.2007.01727.x).
- Barros, A. P., and G. J. Bowden, 2008: Toward long-lead operational forecasts of drought: An experimental study in the Murray–Darling River basin. *J. Hydrol.*, **357**, 349–367, doi:[10.1016/j.jhydrol.2008.05.026](https://doi.org/10.1016/j.jhydrol.2008.05.026).
- Bell, V. A., H. N. Davies, A. L. Kay, T. J. Marsh, A. Brookshaw, and A. Jenkins, 2013: Developing a large-scale water-balance approach to seasonal forecasting: Application to the 2012 drought in Britain. *Hydrol. Processes*, **27**, 3003–3012, doi:[10.1002/hyp.9863](https://doi.org/10.1002/hyp.9863).
- Bowling, L. C., and D. P. Lettenmaier, 2010: Modeling the effects of lakes and wetlands on the water balance of Arctic environments. *J. Hydrometeor.*, **11**, 276–295, doi:[10.1175/2009JHM1084.1](https://doi.org/10.1175/2009JHM1084.1).
- Ciais, P., and Coauthors, 2005: Europe-wide reduction in primary productivity caused by heat and drought in 2003. *Nature*, **437**, 529–533, doi:[10.1038/nature03972](https://doi.org/10.1038/nature03972).
- Dutra, E., L. Magnusson, F. Wetterhall, H. L. Cloke, G. Balsamo, S. Bousetta, and F. Pappenberger, 2013: The 2010–2011 drought in the Horn of Africa in ECMWF reanalysis and seasonal forecast products. *Int. J. Climatol.*, **33**, 1720–1729, doi:[10.1002/joc.3545](https://doi.org/10.1002/joc.3545).
- Ek, M. B., K. E. Mitchell, Y. Lin, E. Rogers, P. Grunmann, V. Koren, G. Gayno, and J. D. Tarpley, 2003: Implementation of Noah land surface model advances in the National Centers for Environmental Prediction operational mesoscale Eta model. *J. Geophys. Res.*, **108**, 8851, doi:[10.1029/2002JD003296](https://doi.org/10.1029/2002JD003296).
- Guo, Z., and P. A. Dirmeyer, 2013: Interannual variability of land–atmosphere coupling strength. *J. Hydrometeor.*, **14**, 1636–1646, doi:[10.1175/JHM-D-12-0171.1](https://doi.org/10.1175/JHM-D-12-0171.1).
- Higgins, R. W., W. Shi, E. Yarosh, and R. Joyce, 2000: *Improved United States Precipitation Quality Control System and Analysis*. NCEP/Climate Prediction Center Atlas 7, 40 pp.
- Hoerling, M., and A. Kumar, 2003: The perfect ocean for drought. *Science*, **299**, 691–694, doi:[10.1126/science.1079053](https://doi.org/10.1126/science.1079053).
- , J. Eischeid, A. Kumar, R. Leung, A. Mariotti, K. Mo, S. Schubert, and R. Seager, 2014: Causes and predictability of the 2012 Great Plains drought. *Bull. Amer. Meteor. Soc.*, **95**, 269–282, doi:[10.1175/BAMS-D-13-00055.1](https://doi.org/10.1175/BAMS-D-13-00055.1).
- Hunt, E., M. Svoboda, B. Wardlow, K. Hubbard, M. J. Hayes, and T. Arkebauer, 2014: Monitoring the effects of rapid onset of drought on non-irrigated maize with agronomic data and climate-based drought indices. *J. Agric. For. Meteor.*, **191**, 1–11, doi:[10.1016/j.agrformet.2014.02.001](https://doi.org/10.1016/j.agrformet.2014.02.001).
- Hwang, Y., and G. Carbone, 2009: Ensemble forecasts of drought indices using a conditional resampling technique. *J. Appl. Meteor.*, **48**, 1289–1301, doi:[10.1175/2009JAMC2071.1](https://doi.org/10.1175/2009JAMC2071.1).
- Kebede, H., D. K. Fisher, and L. D. Young, 2012: Determination of moisture deficit and heat stress tolerance in corn using physiological measurements and a low-cost microcontroller-based monitoring system. *J. Agron. Crop Sci.*, **198**, 118–129, doi:[10.1111/j.1439-037X.2011.00493.x](https://doi.org/10.1111/j.1439-037X.2011.00493.x).
- Kim, T. W., J. B. Valdes, and C. Yoo, 2003: Nonparametric approach for estimating return periods of droughts in

- arid regions. *J. Hydrol. Eng.*, **8**, 237–246, doi:[10.1061/\(ASCE\)1084-0699\(2003\)8:5\(237\)](https://doi.org/10.1061/(ASCE)1084-0699(2003)8:5(237)).
- Kirtman, B. P., and Coauthors, 2014: The North American Multi-model Ensemble: Phase-1 seasonal-to-interannual prediction; phase-2 toward developing intraseasonal prediction. *Bull. Amer. Meteor. Soc.*, **95**, 585–601, doi:[10.1175/BAMS-D-12-00050.1](https://doi.org/10.1175/BAMS-D-12-00050.1).
- Koster, R. D., and M. J. Suarez, 1994: The components of a SVAT scheme and their effects on a GCM's hydrological cycle. *Adv. Water Resour.*, **17**, 61–78, doi:[10.1016/0309-1708\(94\)90024-8](https://doi.org/10.1016/0309-1708(94)90024-8).
- , and —, 1996: Energy and water balance calculations in the Mosaic LSM. NASA Technical Report Series on Global Modeling and Data Assimilation, NASA Tech. Memo. TM-104606, Vol. 9, 76 pp. [Available online at <http://gmao.gsfc.nasa.gov/pubs/docs/Koster130.pdf>.]
- Kumar, A., and M. P. Hoerling, 1997: Interpretation and implications of the observed inter-El Niño variability. *J. Climate*, **10**, 83–91, doi:[10.1175/1520-0442\(1997\)010<0083:IAIOTC>2.0.CO;2](https://doi.org/10.1175/1520-0442(1997)010<0083:IAIOTC>2.0.CO;2).
- , M. Chen, M. Hoerling, and J. Eischeid, 2013: Do extreme climate events require extreme forcings? *Geophys. Res. Lett.*, **40**, 3440–3445, doi:[10.1002/grl.50657](https://doi.org/10.1002/grl.50657).
- Li, Y. P., W. Ye, M. Wang, and X. D. Yan, 2009: Climate change and drought: A risk assessment of crop-yield impacts. *Climate Res.*, **39**, 31–46, doi:[10.3354/cr00797](https://doi.org/10.3354/cr00797).
- Liang, X., E. F. Wood, and D. P. Lettenmaier, 1996: Surface and soil moisture parameterization of the VIC-2L model: Evaluation and modifications. *Global Planet. Change*, **13**, 195–206, doi:[10.1016/0921-8181\(95\)00046-1](https://doi.org/10.1016/0921-8181(95)00046-1).
- Loaiciga, H. A., and R. B. Leipnik, 1996: Stochastic renewal model of low-flow streamflow sequences. *Stoch. Hydrol. Hydraul.*, **10**, 65–85, doi:[10.1007/BF01581794](https://doi.org/10.1007/BF01581794).
- Luo, L., and E. F. Wood, 2008: Use of Bayesian merging techniques in a multimodel seasonal hydrologic ensemble prediction system for the eastern United States. *J. Hydrometeor.*, **9**, 866–884, doi:[10.1175/2008JHM980.1](https://doi.org/10.1175/2008JHM980.1).
- , —, and M. Pan, 2007: Bayesian merging of multiple climate model forecasts for seasonal hydrological predictions. *J. Geophys. Res.*, **112**, D10102, doi:[10.1029/2006JD007655](https://doi.org/10.1029/2006JD007655).
- Lyon, B., M. A. Bell, M. K. Tippett, A. Kumar, M. P. Hoerling, X.-W. Quan, and H. Wang, 2012: Baseline probabilities for the seasonal prediction of meteorological drought. *J. Appl. Meteor. Climatol.*, **51**, 1222–1237, doi:[10.1175/JAMC-D-11-0132.1](https://doi.org/10.1175/JAMC-D-11-0132.1).
- Madden, R. A., 1976: Estimates of the natural variability of time-averaged sea-level pressure. *Mon. Wea. Rev.*, **104**, 942–952, doi:[10.1175/1520-0493\(1976\)104<0942:EOTNVO>2.0.CO;2](https://doi.org/10.1175/1520-0493(1976)104<0942:EOTNVO>2.0.CO;2).
- McKee, T. B., N. J. Doesken, and J. Kleist, 1993: The relationship of drought frequency and duration to time scale. *Proc. Eighth Conf. on Applied Climatology*, Anaheim, CA, Amer. Meteor. Soc., 179–184.
- , —, and —, 1995: Drought monitoring with multiple time scales. *Proc. Ninth Conf. on Applied Climatology*, Dallas, TX, Amer. Meteor. Soc., 233–236.
- McNaughton, K. G., and T. W. Spriggs, 1986: A mixed-layer model for regional evaporation. *Bound.-Layer Meteor.*, **34**, 243–262, doi:[10.1007/BF00122381](https://doi.org/10.1007/BF00122381).
- Mesinger, F., and Coauthors, 2006: North American Regional Reanalysis. *Bull. Amer. Meteor. Soc.*, **87**, 343–360, doi:[10.1175/BAMS-87-3-343](https://doi.org/10.1175/BAMS-87-3-343).
- Mishra, V. R., and A. K. Desai, 2005: Drought forecasting using stochastic models. *Stochastic Environ. Res. Risk Assess.*, **19**, 326–339, doi:[10.1007/s00477-005-0238-4](https://doi.org/10.1007/s00477-005-0238-4).
- , and —, 2006: Drought forecasting using feed-forward recursive neural network. *Ecol. Model.*, **198**, 127–138, doi:[10.1016/j.ecolmodel.2006.04.017](https://doi.org/10.1016/j.ecolmodel.2006.04.017).
- , and K. Cherkauer, 2010: Retrospective droughts in the crop growing season: Implications to corn and soybean yield in the Midwestern United States. *Agric. For. Meteor.*, **150**, 1030–1045, doi:[10.1016/j.agrformet.2010.04.002](https://doi.org/10.1016/j.agrformet.2010.04.002).
- Mittler, R., 2006: Abiotic stress, the field environment and stress combination. *Trends Plant Sci.*, **11**, 15–19, doi:[10.1016/j.tplants.2005.11.002](https://doi.org/10.1016/j.tplants.2005.11.002).
- Mozny, M., M. Trnka, Z. Zalud, P. Hlavinka, J. Nekovar, V. Potop, and M. Virág, 2012: Use of a soil moisture network for drought monitoring in the Czech Republic. *Theor. Appl. Climatol.*, **107**, 99–111, doi:[10.1007/s00704-011-0460-6](https://doi.org/10.1007/s00704-011-0460-6).
- Mynden, R. B., and Coauthors, 2002: Global products of vegetation leaf area and fraction absorbed by PAR from year of MODIS data. *Remote Sens. Environ.*, **83**, 214–231, doi:[10.1016/S0034-4257\(02\)00074-3](https://doi.org/10.1016/S0034-4257(02)00074-3).
- Norman, J. M., W. P. Kustas, and K. S. Humes, 1995: A two-source approach for estimating soil and vegetation energy fluxes from observations of directional radiometric surface temperature. *Agric. For. Meteor.*, **77**, 263–292, doi:[10.1016/0168-1923\(95\)02265-Y](https://doi.org/10.1016/0168-1923(95)02265-Y).
- Otkin, J. A., M. C. Anderson, J. R. Mecikalski, and G. R. Diak, 2005: Validation of GOES-based insolation estimates using data from the United States Climate Reference Network. *J. Hydrometeor.*, **6**, 460–475, doi:[10.1175/JHM440.1](https://doi.org/10.1175/JHM440.1).
- , —, C. Hain, I. Mladenova, J. Basara, and M. Svoboda, 2013: Examining flash drought development using the thermal infrared-based evaporative stress index. *J. Hydrometeor.*, **14**, 1057–1074, doi:[10.1175/JHM-D-12-0144.1](https://doi.org/10.1175/JHM-D-12-0144.1).
- , —, —, and M. Svoboda, 2014: Examining the relationship between drought development and rapid changes in the evaporative stress index. *J. Hydrometeor.*, **15**, 938–956, doi:[10.1175/JHM-D-13-0110.1](https://doi.org/10.1175/JHM-D-13-0110.1).
- Özger, M., A. K. Mishra, and V. P. Singh, 2012: Long lead time drought forecasting using a wavelet and fuzzy logic combination model: A case study in Texas. *J. Hydrometeor.*, **13**, 284–297, doi:[10.1175/JHM-D-10-05007.1](https://doi.org/10.1175/JHM-D-10-05007.1).
- Pan, M., X. Yuan, and E. F. Wood, 2013: A probabilistic framework for assessing drought recovery. *Geophys. Res. Lett.*, **40**, 3637–3642, doi:[10.1002/grl.50728](https://doi.org/10.1002/grl.50728).
- Pozzi, W., and Coauthors, 2013: Toward global drought early warning capability. *Bull. Amer. Meteor. Soc.*, **94**, 776–785, doi:[10.1175/BAMS-D-11-00176.1](https://doi.org/10.1175/BAMS-D-11-00176.1).
- Pradhan, G. P., P. V. V. Prasad, A. K. Fritz, M. B. Kirkham, and B. S. Gill, 2012: Response of *Aegilops* species to drought stress during reproductive stages of development. *Funct. Plant Biol.*, **39**, 51–59, doi:[10.1071/FP11171](https://doi.org/10.1071/FP11171).
- Prasad, P. V. V., S. R. Pisipati, I. Momcilovic, and Z. Ristic, 2011: Independent and combined effects of high temperature and drought stress during grain filling on plant yield and chloroplast EF-Tu expression in spring wheat. *J. Agron. Crop Sci.*, **197**, 430–441, doi:[10.1111/j.1439-037X.2011.00477.x](https://doi.org/10.1111/j.1439-037X.2011.00477.x).
- Quan, X.-W., M. P. Hoerling, B. Lyon, A. Kumar, M. A. Bell, M. K. Tippett, and H. Wang, 2012: Prospects for dynamical prediction of meteorological drought. *J. Appl. Meteor. Climatol.*, **51**, 1238–1252, doi:[10.1175/JAMC-D-11-0194.1](https://doi.org/10.1175/JAMC-D-11-0194.1).
- Rötter, R., and S. C. van de Geijn, 1999: Climate change effects on plant growth, crop yield, and livestock. *Climatic Change*, **43**, 651–681, doi:[10.1023/A:1005541132734](https://doi.org/10.1023/A:1005541132734).
- Saini, H. S., and M. E. Westgate, 1999: Reproductive development in grain crops during drought. *Adv. Agron.*, **68**, 59–96, doi:[10.1016/S0065-2113\(08\)60843-3](https://doi.org/10.1016/S0065-2113(08)60843-3).
- Schubert, S. D., M. J. Suarez, P. J. Pegion, R. D. Koster, and J. T. Bacmeister, 2004: Causes of long-term drought in the

- U.S. Great Plains. *J. Climate*, **17**, 485–503, doi:[10.1175/1520-0442\(2004\)017<0485:COLDIT>2.0.CO;2](https://doi.org/10.1175/1520-0442(2004)017<0485:COLDIT>2.0.CO;2).
- , R. Koster, M. Hoerling, R. Seager, D. Lettenmaier, A. Kumar, and D. Gutzler, 2007: Predicting drought on seasonal-to-decadal time scales. *Bull. Amer. Meteor. Soc.*, **88**, 1625–1630, doi:[10.1175/BAMS-88-10-1625](https://doi.org/10.1175/BAMS-88-10-1625).
- Sen, Z., and V. K. Boken, 2005: Techniques to predict agricultural droughts. *Monitoring and Predicting Agricultural Drought*, V. K. Boken, A. P. Cracknell, and R. L. Heathcote, Eds., Oxford University Press, 40–54.
- Steinemann, A., 2003: Drought indicators and triggers: A stochastic approach to evaluation. *J. Amer. Water Resour. Assoc.*, **39**, 1217–1233, doi:[10.1111/j.1752-1688.2003.tb03704.x](https://doi.org/10.1111/j.1752-1688.2003.tb03704.x).
- Svoboda, M., and Coauthors, 2002: The Drought Monitor. *Bull. Amer. Meteor. Soc.*, **83**, 1181–1190.
- Swain, S., B. D. Wardlow, S. Narumalani, T. Tadesse, and K. Callahan, 2011: Assessment of vegetation response to drought in Nebraska using Terra-MODIS land surface temperature and normalized difference vegetation index. *GISci. Remote Sens.*, **48**, 432–455, doi:[10.2747/1548-1603.48.3.432](https://doi.org/10.2747/1548-1603.48.3.432).
- USDA, 2013: Crop production: 2012 summary. USDA Rep., 95 pp. [Available online at <http://usda01.library.cornell.edu/usda/nass/CropProdSu/2010s/2013/CropProdSu-01-11-2013.pdf>.]
- Wei, H., Y. Xia, K. E. Mitchell, and M. B. Ek, 2013: Improvement of the Noah land surface model for warm season processes: Evaluation of water and energy flux simulation. *Hydrol. Processes*, **27**, 297–303, doi:[10.1002/hyp.9214](https://doi.org/10.1002/hyp.9214).
- Wilks, D. S., 2011: *Statistical Methods in the Atmospheric Sciences*. 3rd ed. International Geophysics Series, Vol. 100, Academic, 676 pp.
- Wood, A. W., E. P. Maurer, A. Kumar, and D. P. Lettenmaier, 2002: Long range experimental hydrologic forecasting for the eastern U.S. *J. Geophys. Res.*, **107**, 4429, doi:[10.1029/2001JD000659](https://doi.org/10.1029/2001JD000659).
- Xia, Y., M. B. Ek, H. Wei, and J. Meng, 2012a: Comparative analysis of relationships between NLDAS-2 forcings and model outputs. *Hydrol. Processes*, **26**, 467–474, doi:[10.1002/hyp.8240](https://doi.org/10.1002/hyp.8240).
- , and Coauthors, 2012b: Continental-scale water and energy flux analysis and validation of the North American Land Data Assimilation System project phase 2 (NLDAS-2): 1. Intercomparison and application of model products. *J. Geophys. Res.*, **117**, D03109, doi:[10.1029/2011JD016048](https://doi.org/10.1029/2011JD016048).
- , J. Sheffield, M. B. Ek, J. Dong, N. Chaney, H. Wei, J. Meng, and E. F. Wood, 2014: Evaluation of multi-model simulated soil moisture in NLDAS-2. *J. Hydrol.*, **512**, 107–125, doi:[10.1016/j.jhydrol.2014.02.027](https://doi.org/10.1016/j.jhydrol.2014.02.027).
- Yuan, X., and E. F. Wood, 2013: Multimodel seasonal forecasting of global drought onset. *Geophys. Res. Lett.*, **40**, 4900–4905, doi:[10.1002/grl.50949](https://doi.org/10.1002/grl.50949).
- , —, N. W. Chaney, J. Sheffield, J. Kam, M. Liang, and K. Guan, 2013: Probabilistic seasonal forecasting of African drought by dynamic models. *J. Hydrometeorol.*, **14**, 1706–1720, doi:[10.1175/JHM-D-13-054.1](https://doi.org/10.1175/JHM-D-13-054.1).